

Vacancy induced magnetism in graphene and graphene ribbons

J. J. Palacios and J. Fernández-Rossier

*Departamento de Física Aplicada, Universidad de Alicante,
San Vicente del Raspeig, E-03690 Alicante, Spain.*

L. Brey

Instituto de Ciencia de Materiales de Madrid, Consejo Superior de Investigaciones Científicas, E-28049 Cantoblanco, Spain

(Dated: October 8, 2018)

We address the electronic structure and magnetic properties of vacancies and voids both in graphene and graphene ribbons. Using a mean field Hubbard model, we study the appearance of magnetic textures associated to removing a single atom (vacancy) and multiple adjacent atoms (voids) as well as the magnetic interactions between them. A simple set of rules, based upon Lieb theorem, link the atomic structure and the spatial arrangement of the defects to the emerging magnetic order. The total spin S of a given defect depends on its sublattice imbalance, but some defects with $S = 0$ can still have local magnetic moments. The sublattice imbalance also determines whether the defects interact ferromagnetically or antiferromagnetically with one another and the range of these magnetic interactions is studied in some simple cases. We find that in semiconducting armchair ribbons and two-dimensional graphene without global sublattice imbalance there is maximum defect density above which local magnetization disappears. Interestingly, the electronic properties of semiconducting graphene ribbons with uncoupled local moments are very similar to those of diluted magnetic semiconductors, presenting giant Zeeman splitting.

PACS numbers:

I. INTRODUCTION

Magnetic order occurs, in most instances, in materials with partially filled d or f shells. There is, however, a recent awareness that the possibility of magnetic order can also occur in materials without open d or f shells^{1,2,3,4,5}. Experimental evidence of this new type of magnetism has been found in thin films of certain oxides (HfO₂, ZnO, TiO₂)¹, as well as irradiated graphite², and thiol-capped gold nanoparticles^{6,7}.

Although more experimental work is probably necessary to confirm and understand magnetism in these systems, there are at least two scenarios for which theory provides a mechanism for the appearance of magnetism without d or f open shells. On one side, in some lattices intrinsic lattice defects like vacancies lead to the formation local magnetic moments, a preliminary condition for the existence of magnetic order. This is the case in graphite⁸, graphene^{9,10,11} and II-VI semiconductors¹². On the other side, it has been recently found that clusters with specific shapes, like triangular graphene islands³ or icosahedral^{4,5} gold clusters, have large degeneracies at the Fermi energy in their single particle spectra. These degeneracies are related to the symmetry of the nanostructure and, in words of Luo *et al.*⁵, they behave like 'superatoms', with magnetic ground states that comply with atomic-like Hund's rules.

Importantly, both vacancy induced^{10,11} and 'superatomic' magnetism³ occur in graphene structures and, as we show here, have the same origin. In this work we present extensive numerical work to understand vacancy induced magnetism in graphene and graphene ribbons and we analyze our results in the context of a

broader theoretical framework that unifies superatomic³ and vacancy induced magnetism^{10,11} in graphene. In part our motivation stems from the recently shown possibility of fabricating high mobility graphene based field effect transistors^{13,14,15,16,17,18} which has created enormous interest in graphene based electronics¹⁹. Additional possibilities arise from the fabrication of semiconducting graphene ribbons^{20,21,22} and graphene nanoislands^{19,23} with top-down techniques as well as the growth of graphene islands with bottom-up techniques^{24,25}. Magnetic order in patterned or nanostructured graphene would bring up new opportunities of research in spintronics.

Graphene honeycomb structure is a bipartite lattice, formed by two interpenetrating triangular sublattices, A and B, such that the first neighbors of an atom A belong to the sublattice B and viceversa²⁶. The low-energy electronic structure of graphene can be described by a single-orbital (p_z) nearest-neighbor hopping Hamiltonian^{26,27}. This model correctly describes two dimensional graphene as a zero gap semiconductor with linear bands around the Fermi energy. The single particle spectrum of a nearest-neighbor tight-binding model in a bipartite lattice has particle-hole symmetry^{28,29}.

The magnetic properties of both graphene-based nanostructures and defective graphene are intimately related to the appearance of midgap states and how they are affected by electron-electron interactions. The existence of zero-energy states in disordered bipartite lattices was proved by Inui *et al.*²⁸. Within the first-neighbor tight-binding model, a sufficient condition^{3,28} for the existence of midgap states is the existence of a finite sublattice imbalance, $N_I \equiv N_A - N_B$, where N_A and N_B are the number of atoms belonging to each sublattice or miss-

ing from each sublattice in an otherwise perfect system. Thus, whereas ideal graphene has $N_I = 0$ and no midgap states, both defective graphene and some graphene islands, such as triangles, can present finite sublattice imbalance and $|N_I|$ midgap states. The result of Inui *et al.*²⁸ has been used in a recent work on disorder in graphene by Pereira *et al.*³⁰. Incidentally, the existence of zero-energy or midgap states in uncompensated graphene structures was known long ago in the context of chemical studies of hydrocarbons as the Longuet-Higgis conjecture³¹.

Because of the particle-hole symmetry, midgap states are half filled for neutral graphene and the appearance of magnetic moments is expected in analogy with Hund's rule in atomic magnetism. The Hubbard model extends the single-particle tight-binding model including the effect of Coulomb repulsion between two electrons in the same atomic site. Importantly, a theorem by Lieb, valid for the exact ground state of the Hubbard model and neutral bipartite lattices³² states that the total spin S of the ground state is given by $2S = |N_A - N_B| = |N_I|$. Lieb's theorem provides a rigorous connection between vacancies in the graphene lattice and the emergence of magnetism. As a result, sublattice unbalanced neutral graphene will always present a finite total magnetic moment.

Although Lieb's theorem provides the total spin of the ground state, it does not say much about the actual local magnetic order or spin texture. For instance, $S = 0$ does not preclude the existence of local magnetic moments coupled antiferromagnetically or presenting compensated ferrimagnetic order. The most notorious example of compensated ferrimagnetic order can be found in zigzag ribbons^{33,34,35,36,37}, where each edge presents ferromagnetic order antiparallel to each other for a total vanishing magnetic moment. Other examples can be found in hexagonal graphene islands, where, beyond a critical size, contiguous sides alternate the direction of the ferromagnetically ordered magnetic moments³.

The rest of this paper is organized as follows. In Sec. II we review the single orbital Hubbard model and the different methodologies used to describe the electronic structure of defective graphene and graphene ribbons. The underlying non-interacting spectrum and associated magnetic textures can be anticipated following some basic rules which are presented in Sec. III. We illustrate the validity of the rules by numerical calculations in the case of semiconducting armchair ribbons (Sec. IV) with vacancies, voids, or notches, both in the non-interacting (Sec. IV) and interacting (V) cases. The results for bulk graphene are discussed in Sec. (VI). Summary and conclusions are presented in Sec. VII.

II. METHODOLOGY

We consider the low-energy physics that takes place in the subspace expanded only by the single p_z orbital (the one perpendicular to the graphene plane). Next-

to-neighbor hopping is neglected and the electron-electron interactions are included locally in the form of an on-site repulsion or Hubbard model. When the interactions are turned off this reduces to the widespread one orbital tight-binding model^{27,38,39,40}. The Hubbard term is treated in a mean field approximation^{3,33}. Comparison between the results so obtained and density functional theory (DFT) calculations yield very good agreement for two-dimensional graphene⁴¹, carbon nanotubes^{41,42}, zigzag^{35,37} and armchair graphene ribbons³⁴, as well as graphene islands³.

We model vacancies and voids in perfect graphene or graphene ribbons by removing atoms, actually, by removing the representing p_z orbitals in the tight-binding model. This results in a reduction of the coordination of the atoms adjacent to the missing atoms. We ignore the lattice distortion and we assume that the on-site energy is the same for edge and bulk atoms. The single-orbital hamiltonian implicitly assumes full hydrogen passivation of the sp_2 dangling bonds of the atoms without full coordination. This assumption, which might not be completely realistic in the case of actual vacancies⁸, does not invalidate our model; for we can consider an alternative physical realization: The chemisorption of a hydrogen atom on top of a bulk graphene atom¹¹ effectively removes a p_z orbital from the low-energy hamiltonian. In our one-orbital model there is no difference between these two scenarios.

DFT calculations on graphene ribbons^{34,36}, graphene islands^{3,46,50}, and bulk graphene with vacancies¹¹ have shown that the results follow the predictions of Lieb's theorem, even though DFT calculations go beyond the first-neighbor hopping, short-range interaction Hubbard model on which the theorem is based. In other words, second neighbour hopping and inter-site Coulomb repulsion, present in the DFT calculations, do not modify the relation between lattice imbalance and total spin of the ground state warranted for the Hubbard model for which these couplings are absent. From this point of view these couplings are irrelevant. It is thus justified to consider the following mean-field hamiltonian:

$$H = H_0 + U \sum_i (n_{i\uparrow} \langle n_{i\downarrow} \rangle + n_{i\downarrow} \langle n_{i\uparrow} \rangle) - U \sum_i \langle n_{i\downarrow} \rangle \langle n_{i\uparrow} \rangle, \quad (1)$$

where i runs over all lattice sites and the non-interacting hamiltonian reads

$$H_0 = \sum_{i,j} t (c_i^\dagger c_j + c_j^\dagger c_i), \quad (2)$$

where the sum runs over nearest-neighbor lattice sites i, j and $t = 2.5$ eV. Without loss of generality, we have set the diagonal terms of the Hamiltonian to zero. For neutral graphene we can rewrite the mean-field hamiltonian (up to a constant) as the sum of two terms:

$$H = H_0 + \frac{U}{2} \sum_i n_i \langle n_i \rangle - U \sum_i 2m_i \langle m_i \rangle \quad (3)$$

where $m_i = \frac{1}{2}(n_{i\uparrow} - n_{i\downarrow})$ and $n_i = n_{i\uparrow} + n_{i\downarrow}$. The second term in \hat{H} represents the non-trivial contribution of interactions.

The calculations have been performed considering three different types of boundary conditions. For the evaluation of the non-interacting density of states (DOS) in ribbons we compute the Green's function projected on the region where the defects are located. The perfect regions of the ribbon away from the defects are included in the Green's function by means of a self-energy. We refer the reader to Ref. 40 for more details on this methodology. When the interactions are turned on ($U \neq 0$) we consider ribbons with periodic boundary conditions in one direction or, for bulk graphene, periodic boundary conditions in both directions. More details will be given in the respective sections.

III. BASIC RULES

In this section we provide some general rules to understand the appearance of midgap states and magnetic textures due to single-atom vacancies or, more generally, voids in an otherwise sublattice balanced graphene structure, for instance, an infinite defect-free semiconducting armchair ribbon. A void in graphene can be partially characterized by the number and type, A or B, of atoms removed from the otherwise perfect structure. We will label voids as one would do for chemical compounds, $A_{N_A}B_{N_B}$. Voids will be unbalanced when they are created by removing N_A and N_B atoms such that $N_I = N_A - N_B \neq 0$. The sublattice imbalance N_I , which can be either positive or negative, can be interpreted as an imbalance "charge". This quantity is central to our discussion, although the exact formula of the void is also important since it gives an idea of the size and shape of the void. In the case of ribbons the voids can be close to the edges, becoming thus notches. (For the most part we will refer to voids in the bulk of the ribbon, but the conclusions apply equally to the case of notches on the edges.) For a single unbalanced void characterized by N_I , $|N_I|$ zero-energy states appear in the non-interacting spectrum with weight on only one sublattice²⁸. When the graphene structure presents a gap E_g , as in armchair ribbons, these states are normalizable and localized around the void (in contrast to two-dimensional graphene where the zero-energy states are not normalizable⁵¹). Figure 1 shows various examples of voids in a ribbon with different sublattice imbalance N_I .

Let us consider now two voids, characterized *locally* by $N_I(1)$ and $N_I(2)$, sufficiently separated so that they do not affect each other. According to the result of Inui et al.²⁸, the single particle spectrum has, at least,

$$N_Z^{\min} = |N_I(1) + N_I(2)| \quad (4)$$

midgap states. The important question is what happens when the distance between them is such that they do affect each other. If $N_I(1)$ and $N_I(2)$ have the same

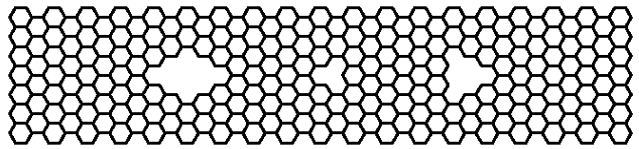


FIG. 1: Examples of voids with different sublattice imbalance in the middle of a graphene ribbon. From left to right the associated imbalance charge is $N_I = 0, -1$ (vacancy), and 2.

sign, there are $|N_I(1)| + |N_I(2)|$ midgap states, regardless of the distance. If they have different signs, e.g., $N_I(1) + N_I(2) = 0$, Eq. 4 apparently warrants the annihilation of midgap states. Within the non-interacting model midgap states are 100 percent sublattice polarized. The non-interacting Hamiltonian has finite matrix elements between states that have weight on different sublattices. Hence, the mechanism for midgap state annihilation is hybridization of midgap states localized in different sublattices. This annihilation occurs as bonding-antibonding pairs of midgap states form, resulting in a shift in their energy and in a loss of the sublattice polarization. For large distances, however, this annihilation does not occur.

A well understood related example occurs in zigzag ribbons^{38,39}. The edge of a zigzag ribbon has a local sublattice imbalance. If the top edge belongs to the A sublattice, the bottom edge belongs to the B sublattice. States fully localized in the edge have zero energy and are localized in a single sublattice. To the extent that states mostly localized on the top edge penetrate into the ribbon, they hybridize with states mostly localized on the bottom edge. This mixing results in a bonding-antibonding splitting that takes these states away from the Dirac energy. In the case of zigzag ribbons, the degree of localization in the unit cell depends on the wavevector. States close to the zone boundary are very localized in the edges and have energy very close to zero^{38,39}. The localization decreases as the wavevector departs from the boundary, resulting in the hybridization and the departure from zero energy³⁸.

In the general case one can conclude that the minimum number of zero-energy states will be given by

$$N_Z^{\min} = \sum_{\alpha, \beta} |N_I(\alpha) + N_I(\beta)|, \quad (5)$$

where the integer indices α and β run over voids with the same imbalance sign, respectively. In practice, within an arbitrarily small energy interval $|E| \rightarrow 0$, the number of zero-energy states can be as large as

$$N_Z^{\max} = \sum_{\alpha} |N_I(\alpha)| + \sum_{\beta} |N_I(\beta)|. \quad (6)$$

In the general case, N_Z will be a number between N_Z^{\min} and N_Z^{\max} .

When electron-electron interactions are turned on, at least locally in the form of a Hubbard-type interaction, Lieb's theorem guarantees that $|N_I| = 2S$ for neutral graphene. The theorem, however, does not exclude the possibility of spin-symmetry broken local magnetic order when $S = 0$ or small. For instance, two or more voids with local sublattice imbalances that cancel out the total imbalance can still retain their local magnetic order when they are not in proximity. When the imbalance of the void is zero but the size is large an internal ferrimagnetic order cannot be discarded either. In general, calculations will be necessary to ascertain the spin texture in these situations. A few conclusions, however, can be reached without actually performing any calculations. One can distinguish four cases:

1. $N_Z^{min} = N_Z = N_Z^{max}$: In this case all the voids are of the same sign. The coupling between them is always ferromagnetic and the spin of the ground state is $2S = N_Z$. The splitting with smaller spin states will depend on the inter-void coupling.
2. $N_Z^{min} = N_Z < N_Z^{max}$: In this case all the voids of different sign are in proximity and interact, yielding a $2S = N_Z^{min}$ state. Calculations will be necessary to ascertain the spin texture in these situations.
3. $N_Z^{min} < N_Z = N_Z^{max}$: In this case all the voids of different type are separated and uncoupled. The ground state has $2S = N_Z^{min}$, but the spin-flip gap is negligible since there are uncoupled magnetic moments.
4. $N_Z^{min} < N_Z < N_Z^{max}$: In this case there are voids of different sign, but some of them are uncoupled and some not. This is the most general case. The ground state has $2S = N_Z^{min}$, but, as in the previous case, the spin-flip gap is negligible since there are uncoupled magnetic moments. Calculations will be necessary to ascertain the spin texture in these situations as well.

IV. DEFECTS IN SEMICONDUCTING GRAPHENE RIBBONS: NON-INTERACTING THEORY

In this section we study the electronic structure of defective graphene ribbons within the non-interacting tight-binding model. The results are obtained using the cluster embedded method described in Ref. 40. In this methodology a finite portion of the ribbon containing the defects is attached to two semi-infinite perfect ribbons of the same width and compute the DOS of the defective region. In the defect free case we obtain a gap in the DOS. We consider armchair graphene ribbons of width $W = N_y a$, where N_y is an integer number and $a = 2.42$ Å is the graphene lattice parameter. We only consider values of W such that, within the first-neighbor tight-binding model, the ribbon is semiconducting^{38,39}. This

happens if $N_y + 1$ is not a multiple of three. More realistic calculations³⁴ predict that, because of lattice distortion of the edge atoms, even ribbons with $N_y + 1 = 3m$, where m is an integer, are semiconductors. Semiconducting graphene ribbons attract interest due to possible applications in nanoelectronics^{20,21,43,44}. As in the case of Si based semiconductors, their electronic structure might be strongly influenced by impurities. Here we study the effect of vacancies and voids, which are expected to act as neutral impurities.

A. Single void

The simplest defective structure is a perfect semiconducting graphene ribbon from which a single atom, A or B, is removed. In agreement to Eq. 4, a zero energy state appears in the DOS. For neutral graphene, this state is half filled. In other words, an spin unpaired electron occupies the midgap state. The local density of states at zero energy, which is nothing but the modulus square of the wave function associated with the zero energy state, is shown in the inset of Fig. 2(a). The state is localized in the neighborhood of the vacancy. The shape of the midgap state is also peculiar: It has a clear directionality. Monoatomic vacancies have the shape of a triangle. Two vertices of the triangle point towards the edges of the ribbon, whereas the lateral vertex can point downstream or upstream along the ribbon. The midgap state is peaked around the lateral vertex. Hence, midgap states have a strong directional character.

Importantly, the *integrated* charge, including both midgap and band states below the Fermi energy, yields a homogeneous charge distribution: there is one electron per atom in every atom, even in the presence of the vacancy. Hence, the localized midgap state does not imply charge localization, yet there is a finite spin density. The total spin S of the neutral graphene with one vacancy is $1/2$ and the spin density does show a non-homogeneous texture, as shown in Fig. 2(a). Hence, the region of the material around the defect has no local charge but has local spin.

Our next step is to consider larger voids. In Fig. 2(b) we show the results for a void with $N_I = 2$, obtained by removing four atoms (A_3B_1). In agreement to Eq. 4, there are two midgap states (per spin). Their local density of states is shown in the inset of Fig. 2(b). As in the case of monoatomic vacancy, two electrons occupy the midgap states. The *integrated* local charge is also homogeneous: One electron per site. Within the framework of the non-interacting model we cannot discriminate between the $S = 0$ or the $S = 1$. As we discuss below, when Hubbard repulsion is turned on Lieb's theorem warrants that the spin of this structure is $S = 1$. In Fig. 2(b) we show the magnetization density, calculated including the interactions, as discussed below. As in the case of a single missing atom, there is a magnetic texture with $S = 1$ which is localized in a region without local-

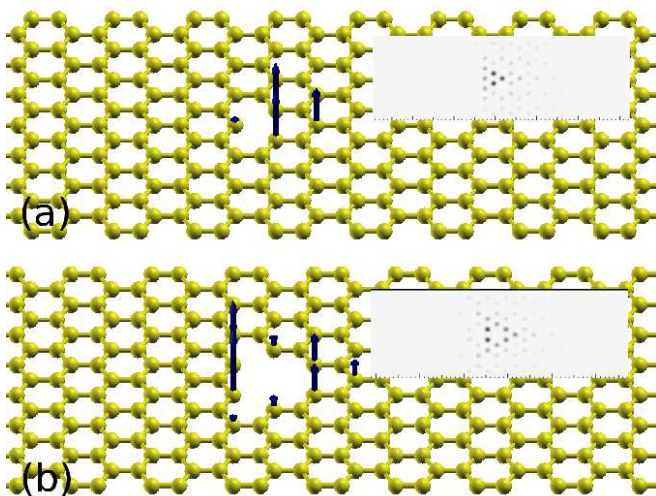


FIG. 2: (Color online) (a) Magnetic moments on lattice sites around a single vacancy. Inset: Probability density of the zero-energy state built with gaussian functions on lattice sites. (b) Same as in (a) but for a triangular void with $N_I = 2$. Inset: Same as in (b) but summing over the two zero-energy states.

ization of extra charge. Triangular voids maximize $|N_I|$ while removing the minimum number of atoms. Larger ones ($|N_I| > 2$) exhibit similar features to the ones already discussed. More complicated voids with zig-zag edges such as hexagons or rombi, which have $N_I = 0$, can still present quasi zero-energy states if they are sufficiently big and therefore might exhibit spin textures as discussed below.

B. Two voids

As a step towards understanding the electronic structure of graphene with a finite density of defects, we first consider the electronic structure of two voids with the same absolute value of N_I . Each void has a well defined sublattice imbalance number N_I when apart, which can be positive or negative. If the sublattice imbalance of the two voids has the same sign, the global structure has twice as many zero energy states as the separated defects. The non-interacting hamiltonian does not couple sites on the same sub-lattices so that the zero-energy states associated with two vacancies with sublattice imbalance of the same sign cannot interact, regardless of the distance separating them, i.e., the non-interacting DOS will always present a delta function at zero energy that can accomodate $2 \times |N_I|$ electrons per spin channel.

When the imbalance numbers are of different sign they cancel out each other. When the defects are far away from each other their local electronic structure is expected to be the same as that of a single defect: Midgap states localized in a single sublattice around the missing atoms. As the defects become closer, the single parti-

cle Hamiltonian, which couples atoms of different sublattices, will hybridize the otherwise sublattice polarized midgap states, which will result in bonding and antibonding pairs away from zero energy. The localization length of the single defect states sets the length scale at which this hybridization occurs.

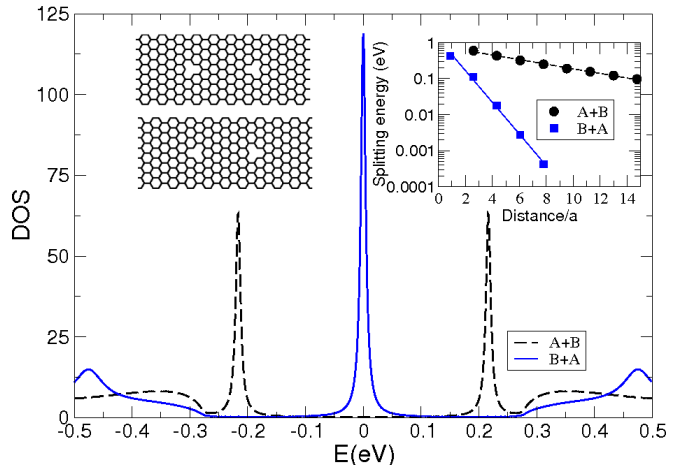


FIG. 3: (Color online) Density of states near the Dirac point for an armchair ribbon of $W = 7a$ with two vacancies presenting charge of different sign and same modulus ($N_I = \pm 1$). Solid lines correspond to the B+A case (left lower inset) and dashed lines correspond to the A+B case (left upper inset). A finite broadening has been added for visibility's sake of the delta functions. The finite, but small, energy splitting in the former case is not visible for this broadening. Right inset: Bonding-antibonding energy splitting as a function of the distance between vacancies for the two different spatial orderings.

Our numerical calculations confirm this scenario. For a given width, the hybridization depends on the distance and, given the directional character of the midgap states in ribbons, on the relative orientation. In Fig. 3 we show the DOS for a system with two monoatomic vacancies A and B ($N_I = \pm 1$, respectively). They are aligned along the ribbon axis and placed at a distance of $6.35a$ away from each other for the two possible spatial orderings, A+B (head to head) and B+A (tail to tail) as shown in the left insets. Due to the high directional character of the associated zero-energy states, the coupling is not invariant against the interchange of positions and the zero-energy states hybridize differently, depending on the spatial ordering. In one case the two-fold zero-energy peak clearly splits into two above and below the Fermi energy. In the other the splitting is much smaller (not visible in this scale). For one relative orientation the wave functions overlap and the degeneracy is strongly removed. For the other the wave functions do not couple at this distance and the degeneracy is practically unaffected. In the right inset of Fig. 3 we show a logarithmic plot of the energy splitting as a function of the distance for the two cases. The splitting decays exponentially in both, reflecting the localized character of the zero-energy

states.

We now consider the case of pairs of defects with larger sublattice imbalance. Figure 4 shows the DOS for two triangular voids characterized by $N_I = +2$ and $N_I = -2$ (A_3B_1 and A_1B_3 , respectively) at different distances. We have selected only one possible ordering in this case (tail to tail). According to these sublattice imbalances each void has associated two localized states. These two states also present a strong directional character, but is different for the two. This can be inferred from the two different bonding-antibonding splitting energies for a given distance seen in Fig. 4. We note that, even when the voids approach each other, the splitting associated with one of the localized states remains small, still being practically zero for small distances. Only in the extreme limit of zero distance when the two voids merge into a single one with sublattice imbalance $N_I = 0$ (A_4B_4) there are no zero-energy states.

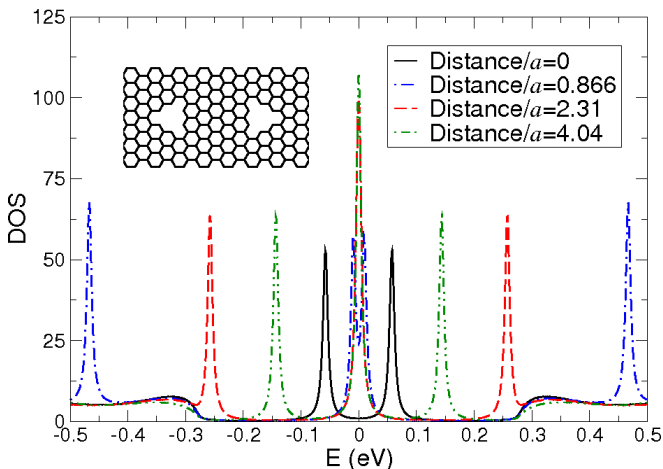


FIG. 4: (Color online) DOS projected on the vicinity of two triangular voids placed along the axis of a semiconducting ribbon for different relative distances. The imbalance charges are the same, but differ in sign ($N_I = \pm 2$).

As the sublattice imbalance of the merging voids becomes bigger and these condense into even bigger $N_I = 0$ voids, the number of states that appear in a vicinity of zero $|E| \rightarrow 0$ increases with the charge of these. Since the appearance of magnetic order relies on the existence of zero-energy states, large voids with $N_I = 0$ can still present ferrimagnetic order, the only condition being that they are formed out of voids with large sublattice imbalance. In other words, their contours must present sufficiently long zig-zag sections. This limits the possible shapes of these voids to, e.g., rombohedral (see Fig. 9) or hexagonal forms. This conclusion is no different from that reached on graphene hexagonal islands³ or finite length ribbons⁴⁶, where calculations have revealed compensated ferrimagnetic order developing along the edge beyond a certain critical size.

Finally, in order to stress the fact that there is nothing in the previous discussion specific to voids in the bulk of

the ribbon, we compute the non-interacting DOS for an A_6B_4 void plus an AB_2 void placed on the edges (i.e., notches) with $N_I = 2$ and $N_I = -1$, respectively. Removing just one atom to create a notch with $N_I = -1$ would have given the same charge as the AB_2 defect, but it would be chemically very unstable and we ignore that possibility. The notches are located on opposite edges, although the results apply the same for notches on the same edge. A single doubly-degenerate state appears at zero energy for the $N_I = 2$ notch. When the second notch is added in close proximity only a single zero-energy state remains, according to the total sublattice imbalance of the system $N_I = 2 - 1 = 1$.

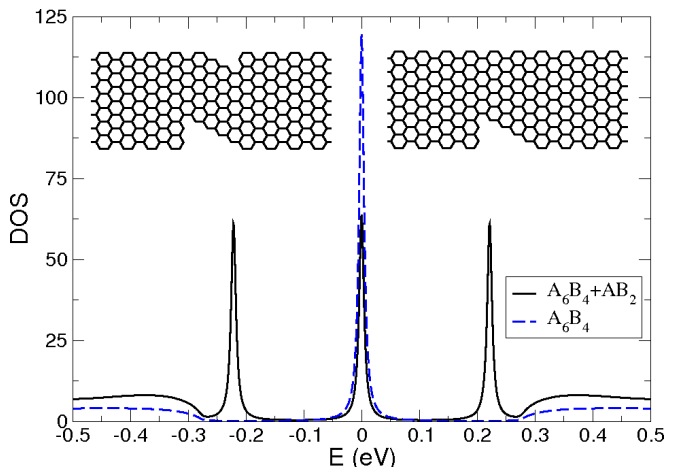


FIG. 5: (Color online) DOS for a single notch with imbalance charge $N_I = 2$ (blue dashed line, right inset). The same notch with an additional notch nearby of charge $N_I = -1$ (black solid line, left inset).

In summary, defective structures with sublattice imbalance result in half-filled midgap states that are expected to yield magnetic moments when interactions are turned on. Structures with global sublattice balance can still present midgap states and be prone to developing local magnetic order, at least in two situations: Distant defects with N_I of opposite sign and large voids with sufficiently long zigzag edges.

V. DEFECTS IN SEMICONDUCTING RIBBONS: INTERACTION EFFECTS

In this section we verify whether the physical picture anticipated from the non-interacting model remains true when the on-site Hubbard repulsions are included. As shown in previous section, unpaired spins appear in sublattice imbalanced structures. When $|N_I| > 1$, the non-interacting model predicts that a shell of $|N_I|$ degenerate mid-gap states is half-filled. The maximization of the spin is expected when Coulomb repulsions are turned on, in the spirit of Hund's rule. At half-filling, the exact ground state of the Hubbard model for a bipartite lattice

such as that of graphene satisfies Lieb's theorem³² which relates the sublattice imbalance and the ground state total spin: $2S = |N_I|$. For unbalanced structures this immediately confirms the Hund's rule scenario. In the case of balanced structures the ground state spin must be zero, but this could happen with local moments, as it happens on the edges of infinite graphene ribbons.

The numerical calculations of this section are done with a unit cell of width W , length $L = N_x \frac{\sqrt{3}}{4} a$, where N_x is the number of carbon atoms along an armchair chain, and with periodic boundary conditions along the x direction to avoid spurious zigzag edges. We consider unit cells as long as 25 nm and the typical number of atoms in a self-consistent calculation is 1000. Importantly, our mean field results have the same relation between the sublattice imbalance and ground state spin than the exact state, as predicted by Lieb theorem.

A. Single void with $U \neq 0$

We first revisit the single void samples. The ground state of structures with single atom vacancies have one unpaired electron within the $U = 0$ model and, according to Lieb's theorem, spin one half in the finite U model. Our mean field calculation, for $U = 2\text{eV}$ agrees with the Lieb theorem. There is a spin splitting of the midgap state Δ_S and a smaller spin splitting δ of the conduction and valence band states, as shown in Fig. 6. The spin degeneracy is thus broken, with only one of the spin channels of the midgap state occupied, the other being empty. This results in a finite magnetization density, localized around the vacancy, as shown in Fig. 2. Although the magnetization resides mostly in the majority sublattice, interactions induce some reversed magnetization in the other sublattice.

1. Analytical model

We can gain some insight by doing an analytical description of the mean field results that involves some approximations valid when U is much smaller than the band-gap of the ideal ribbon E_g . In this case, we assume that only the midgap state is spin polarized:

$$\langle m_i \rangle_0 = \frac{1}{2} |\phi_v(i)|^2 \quad (7)$$

where $|\phi_v(i)|^2$ is the $U = 0$ square modulus of the midgap wave function. Notice that the normalization of $\phi_v(i)$ ensures that the total spin of the ground state is consistent with Lieb's theorem, $\sum_i \langle m_i \rangle_0 = \frac{1}{2}$. The corresponding exchange splitting is

$$\Delta_S = \epsilon_{0\uparrow} - \epsilon_{0\downarrow} = U \sum_i |\phi_v(i)|^2 \langle m_i \rangle_0 = \frac{U}{2} \sum_i |\phi_v(i)|^4 \quad (8)$$

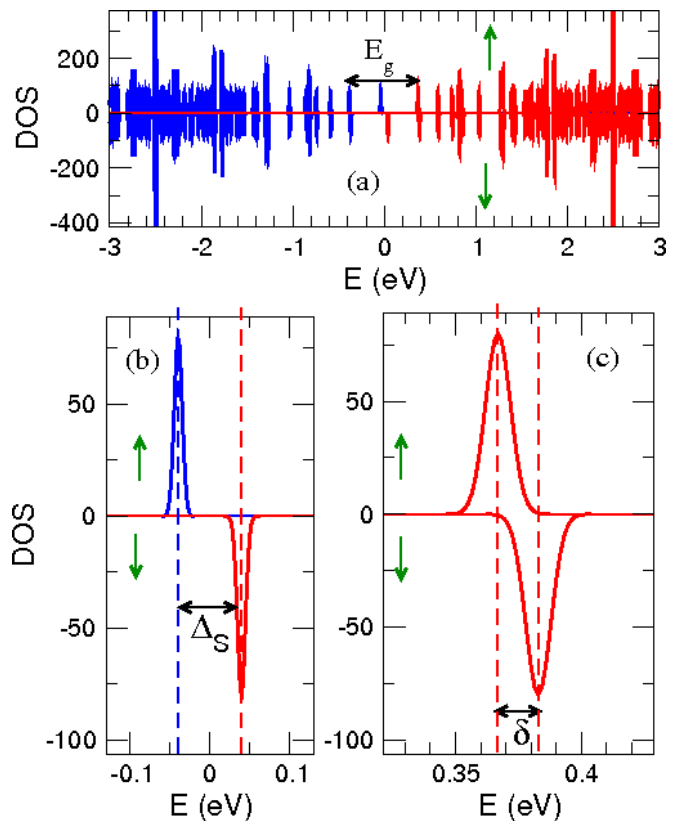


FIG. 6: (Color online) (a) The spin resolved DOS for a ribbon with $W = 7a$ and $U = 2\text{eV}$ with one vacancy. Spin \uparrow (\downarrow) is plotted as a positive (negative) number as a function of energy (we take the Fermi energy as zero). (b) Zoom of the spin-split midgap state. (c) Zoom of the conduction band minima. For clarity, we substitute the delta functions composing the DOS by gaussian functions with a finite broadening.

We see that, within the simplified analytical model, the spin splitting of the midgap state is proportional to the inverse participation ratio, $\eta = \sum_i |\phi_v(i)|^4$. This quantity measures the degree of localization of the zero-energy state. An extended state in which the wave function is equally shared by N atoms, has $\eta = \frac{1}{N^2}$. In the opposite limit where the state is localized in a single atom we would have $\eta = 1$. The inverse participation ratio shown in Fig. 7(c) corresponds to a number of atoms in the range $N = 5$ to $N = 9$. As discussed above, the localization of the midgap states plays an important role in the minimal distance at which they are effectively decoupled.

In Fig. 7(a) we plot the $U = 0$ gap of the ideal ribbon E_g and the $U = 2\text{eV}$ spin splitting Δ_S of the mid-gap state as a function of the ribbon width W , as obtained from the full numerical calculation. As discussed above, we exclude the widths that give $E_g = 0$. We see that the midgap spin splitting is a decreasing function of W . This is related to the fact that, in the small U limit, Δ_S is proportional to the inverse participation ratio η , which is also a decreasing function of the ribbon width, as shown in Fig. 7(c). The extension of the midgap state increases

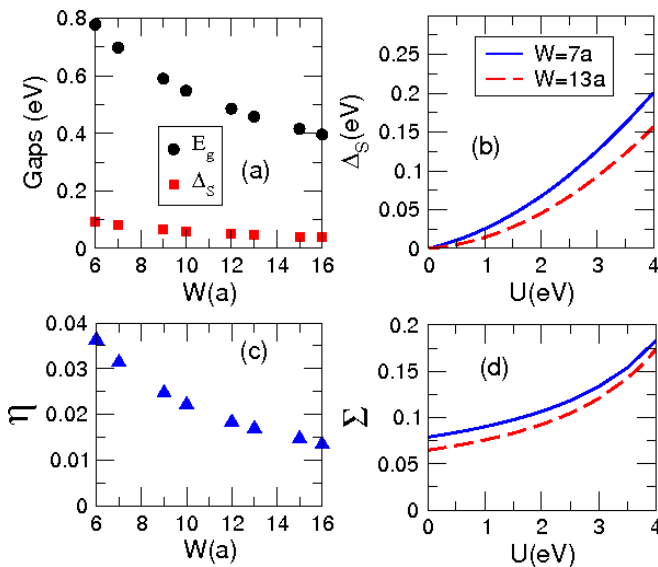


FIG. 7: (Color online) (a) Non-interacting ($U = 0$) energy gap (circles) and interacting ($U = 2\text{eV}$) midgap spin splitting (squares) as a function of the ribbon width W . (b) Midgap spin splitting as a function of U for two ribbon widths $W = 7a$ and $W = 13a$. (c) $U = 0$ inverse participation ratio for the midgap state. (d) Standard deviation of the magnetization Σ , as defined in Eq. 9, as a function of U for two ribbon widths.

as the ribbon becomes wider, resulting in a reduction of the midgap spin splitting. As E_g tends to zero (bulk graphene) the midgap state becomes non-normalizable⁵¹ and Δ_S is expected to vanish (see below).

Whereas the total magnetic moment $\sum_i \langle m_i \rangle$ is given by the sublattice imbalance, the degree of localization of the spin texture is not. In order to quantify it we define the standard deviation

$$\Sigma = \sqrt{\sum_i \langle m_i \rangle^2}. \quad (9)$$

In this definition Σ is not normalized as usual by N , the total number of atoms of the sample, since Σ characterizes a localized object. For sufficiently large simulation cells, doubling N would imply a decrease of a normalized Σ without changing the local properties of the localized magnetic texture. Notice that, within the analytical model valid for $U \ll E_g$, we have $\Sigma \simeq \frac{1}{2}\sqrt{\eta}$. Hence, in the absence of staggered magnetization, both Σ and η would measure the localization of the magnetic moments. For instance, if $\langle m_i \rangle > 0$ at all sites and $S = 1/2$, the maximal Σ would be 0.5. However, the graphene lattice responds with a staggered magnetization to the presence of defects and Σ *also* measures the magnitude of that response. In Figs. 7(b) and (d) we plot the mid-gap spin splitting Δ_S and Σ for two ribbons with $W = 7a$ and $W = 13a$ as a function of U . The midgap spin splittings can be fitted to $\Delta_S(N_y = 7)(U) = 0.0172U + 0.0082U^2$ and to $\Delta_S(N_y = 13)(U) = 0.0062U + 0.00821676U^2$. According to Eq. 8 the linear coefficients should be com-

pared to 0.5η , which is 0.016 for $N_y = 7$ and 0.008 for $N_y = 13$. The non-linear terms arise from the interaction-driven mixing between the midgap states and the conduction states. This is also consistent with the fact that Σ increases as a function of U as shown in the lower panel of Fig. 7(d). The staggered magnetization is an increasing function of U . The coefficient of the quadratic term decreases with the length of the sample, namely, with the distance between vacancies since we are using periodic boundary conditions. We will come back to this issue in the last section.

2. Spin-charge separation for $U > 0$

We have verified that the ground state of structures with single atom vacancies are locally neutral also with $U > 0$: The integrated electronic occupation in every site is one. Hence, a localized spin texture with total spin $1/2$ occurs in the absence of any charge localization. Our numerical results show that the addition of an extra electron to single vacancy structures results in a many electron state with total spin $S = 0$, local magnetization which is zero everywhere, and local charge accumulated in the same atoms and with the same distribution than the magnetic texture of the charge neutral structure. These results are shown in Fig. 8 for a ribbon with $W = 7a$ and $U = 2\text{eV}$. Hence, it is apparent that the monoatomic vacancy results in a multielectronic state with spin charge separation: The neutral ground state has a net electric charge $q = 0$, but a total spin $S = 1/2$ localized in a non-homogeneous spin texture in locally neutral atoms. The charged ground state has a net charge $q = -1$, total spin $S = 0$, no local magnetic moments, and a charge texture localized at the same location than the spin texture of the neutral ground state. This phenomenon resembles that reported by Su-Schrieffer-Heeger⁴⁵ in polyacetylene.

3. Larger voids

We have also calculated the mean field magnetic structure for sublattice imbalanced larger voids. In Fig. 2(b) we show the magnetization profile for a triangular void with $N_I = 2$. For the chosen value of $U = 2\text{eV}$ the staggered magnetization is barely visible in this scale. In agreement with Lieb's theorem, it has a spin $S = 1$, made out of local moments localized, mostly, on the triangle boundaries. This object is the somehow complementary of the triangular graphene islands considered recently by two of us³. Figure 9 shows the ferrimagnetic spin texture around a rhomboidal void with imbalance charge $N_I = 3 - 3 = 0$, i.e., composed of two triangular voids with $N_I = \pm 3$. Local moments with $\langle m_i \rangle \simeq 0.05$, three times smaller than those formed in the edges of infinite length zigzag ribbons, are formed on opposite corners of the void. We have verified that, for $U = 2\text{eV}$, the smallest void of this shape which features local moments is the

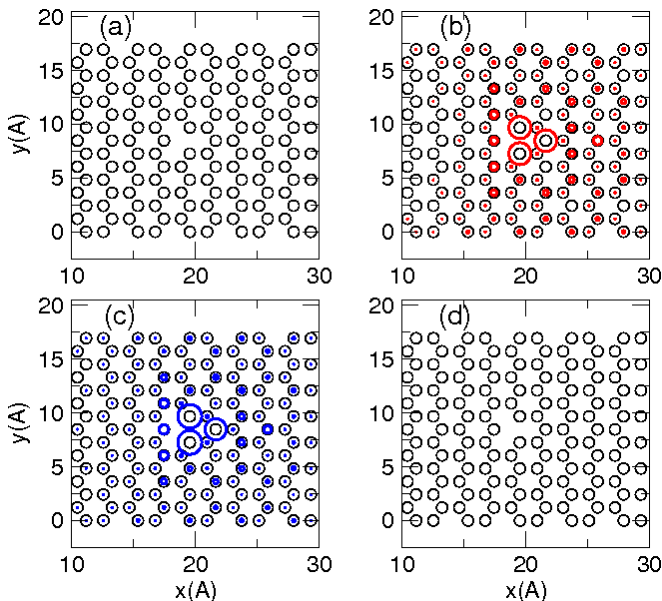


FIG. 8: (Color online) Spin charge separation in single atom vacancy. Left column: neutral case. Right column: Charged case. Upper panels: Charge density $q_i = -1$. Lower panels: $|\langle m_i \rangle| / \sum_i |\langle m_i \rangle|$. The local charge and local spin are zero everywhere for the neutral and charged cases respectively. The spin texture of the neutral case is identical to the charge texture of the charged case.

one of the figure. The rhomboidal void is similar to the hexagonal islands considered in Ref. 3 in the sense that both have $S = 0$ and develop local moments if they are sufficiently large.

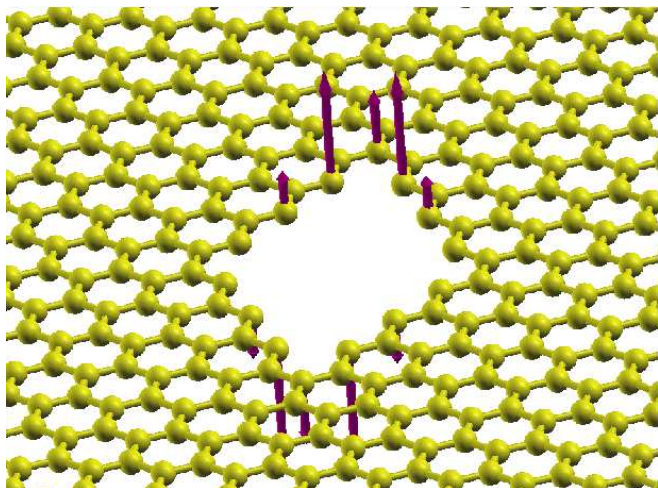


FIG. 9: (Color online) Emerging ferrimagnetic order in a rhombohedral void with imbalance charge $N_I = 3 - 3 = 0$ situated the middle of a ribbon with $W = 10ai$ for $U = 2eV$. The largest magnetic moment per atom is $\langle m_i \rangle = 0.05$

B. Two vacancies with $U \neq 0$

We now study the interaction between two magnetic defects with local sublattice imbalance $N_I = \pm 1$. The Lieb's theorem warrants that, when the sign of the sublattice imbalance is the same for the two defects, the total spin of the ground state is the sum of the spin of the individual defects. Hence, they are coupled *ferromagnetically*^{10,11,47}. In contrast, if the two defects have opposite sublattice imbalance so that the global sublattice imbalance is zero, Lieb's theorem warrants that the total spin is zero. Our calculations show that this can happen in two different scenarios: The local magnetization might be zero everywhere or the two defects could be magnetized along opposite directions, i.e., could be coupled *antiferromagnetically*. When the defects are sufficiently far apart from each other their local electronic structure should be identical to that of single defects. Hence, the spin interaction between two magnetic defects can be either ferromagnetic or antiferromagnetic, as in the case of indirect exchange interactions (RKKY) between single site magnetic moments^{48,49}, but can also result in the annihilation of the local magnetic order, an scenario that goes beyond the RKKY picture.

In Fig. 10 we plot the normalized standard deviation of the two magnetic moments Σ_2 for ribbons with $W = 7a$ and $W = 13a$ as a function of the defect separation. We normalize the computed Σ_2 to the one corresponding to two independent single-defect magnetic textures, $\sqrt{2}\Sigma_1$. Here Σ_1 is the computed single vacancy standard deviation in the same ribbon. When the defects are sufficiently far away Σ_2 must tend to $\sqrt{2}\Sigma_1$, i.e., the normalized Σ_2 must tend to 1. We consider the effect of the ribbon width W , interaction strength U , and sublattice imbalance upon the magnetic interactions between the two defects. In the case of $W = 7a$ we show both monoatomic vacancies lying on the same sublattice (A+A, open circles), whose ground state total spin is $S = 1$, and on different sublattices (A+B, full circles), whose ground state spin is $S = 0$. The two curves for $W = 7a$ are calculated with $U = 2eV$. At large distances, the two defects become decoupled, as expected. At short distances, the behaviour of the magnetic texture is radically different for both A+A and A+B structures. In the former case Σ is enhanced, indicating the localization of the magnetic texture in a smaller region. Since the total spin is 1, local moments survive even when the two defects are very close. As the separation between defects increases they become independent from each other and $\Sigma_2 = \sqrt{2}\Sigma_1$. When this happens, the energy gap between $S = 1$ and $S = 0$ should vanish. This is an example of rule number 1.

In contrast to the A+A case, the *local* magnetization of the A+B structure vanishes below a *minimal distance* D_c . This is an important result. In other words, there is a *maximal density* of defects above which zero energy states hybridize and local magnetic moments vanish. The critical density depends on the energy scales of the prob-

lem, the single particle gap E_g , controlled by the ribbon width, and the on-site repulsion U . For fixed U the decoupling distance is definitely shorter for $W = 7a$ than for $W = 13a$. Hence, the critical (linear) density becomes *smaller*, as the ribbon width *increases*. This is consistent with the fact that both the $U = 0$ inverse participation ratio and the $U \neq 0$ Σ_1 are decreasing functions of the ribbon W . The wider the ribbon, the larger the delocalization of the zero energy state. Hence, the hybridization between the midgap states associated with each vacancy survives at a larger distance for wider ribbons. Finally, in fig. 10 we also show Σ_2 for $W = 13a$ and two values of U , 2 and 4 eV. The decoupling distance (critical density) decreases (increases) as a function of U . In other words, interactions drive the system magnetic, as expected. The A+B case is the simplest example that exemplifies rules number 2 and 3.

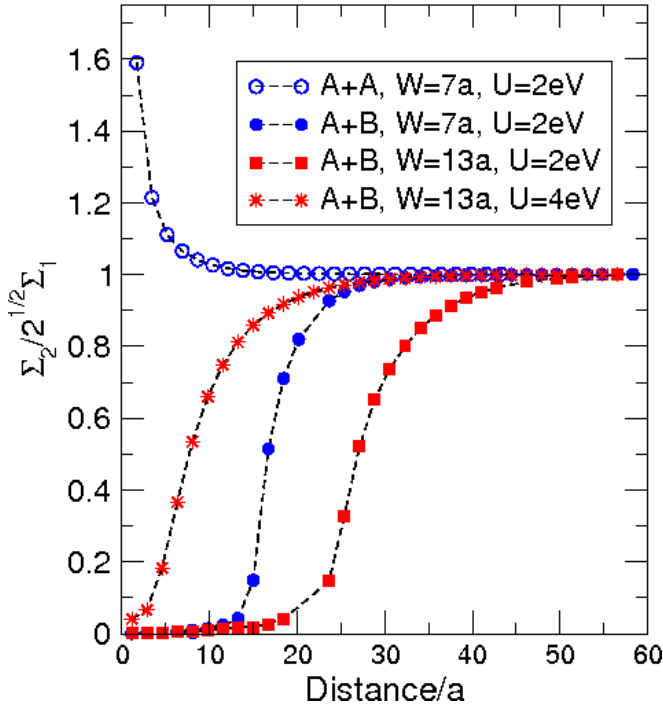


FIG. 10: (Color online) Normalized magnetization as a function of the distance between vacancies for four cases. Ribbon with $W = 7a$, $U = 2\text{eV}$, vacancies in the same sublattice (open circles), same ribbon, holes in different sublattices (full circles), ribbon with $W = 13a$, holes in different sublattices, $U = 2\text{eV}$ (full squares) and $U = 4\text{eV}$ (stars)

According to the two-vacancy calculation shown in the figure, the magnetic (low density, large inter-vacancy distance) and non-magnetic (high density, low inter-vacancy distance) phases are separated by a crossover region. If we take as an estimate of the critical distance below which local moments are quenched the distance for which $\Sigma_2(D_c)/\sqrt{2}\Sigma_1 = 0.5$, we find that $D_c = 40\text{\AA}$ for $W = 7a$ and $D_c = 65\text{\AA}$ for $W = 13a$, both for $U = 2\text{eV}$. The corresponding critical *linear* densities $n_c \equiv \frac{1}{D_c}$ are $n_{1c}(W = 7a) = 2.5 \times 10^6\text{cm}^{-1}$ and $n_{1c}(W = 13a) =$

$1.5 \times 10^6\text{cm}^{-1}$, respectively. The corresponding areal densities, $n_{2c} = \frac{1}{W \times D_c}$ are $n_{2c}(W = 7a) = 1.4 \times 10^{13}\text{cm}^{-2}$ and $n_{2c}(W = 13a) = 4.8 \times 10^{12}\text{cm}^{-2}$ respectively. These numbers should be taken as order of magnitude estimates of the real critical density.

In the case of A+B pairs, the crossover from the locally magnetic to the non-magnetic state is similar to the one described in compensated graphene nanoislands³: Small islands are non-magnetic and larger islands have magnetic edges. The critical density depends on the extension of the magnetization, which in turn, depends on the ribbon single particle gap E_g (which controls the extension of the $U = 0$ midgap states) and on the on-site repulsion U . The quenching of the local moments in the A+B structures is definitely related to the hybridization of the mid-gap states described in the non-interacting model. This phenomenon has an analog in zigzag ribbons. The midgap bands are linear combinations of top and bottom edge states. The hybridization is negligible in the Brillouin zone boundary, and is much larger in the middle. As a result, the exchange interaction strongly renormalize the zone-boundary states, opening a magnetic gap, but they barely change in the middle of the zone³⁷.

C. Defective graphene ribbons as diluted magnetic semiconductors

The physical picture that emerges from the previous discussion leads to an interesting conclusion: A semiconducting graphene ribbon with a density of vacancies that induce magnetism will behave like a diluted (para-)magnetic semiconductor (DMS)⁵² provided that the density of defects is smaller than the critical density defined above (this would be an example of rule number 3). Charged excitations will present a gap and spin excitations will not. The long range ferromagnetic order found by Pisani *et al.* (see Ref. 47) only occurs when the vacancies are all in the same sublattice. It remains an open issue whether or not such a sublattice imbalance might occur in reality. Unless this can be shown, one should not expect long range ferromagnetic order in real samples.

Interestingly, the conduction and valence bands depend on the magnetic order of the local moments, which might be induced by application of an external magnetic field. In the DMS case, the conduction and valence bands are exchanged coupled to the local moments, provided by Mn atoms. At zero field the Mn spins are randomly oriented and the average spin splitting of the bands is zero. Application of an external field orders the Mn spins, resulting in a finite average exchange induced spin splitting of the bands which is much larger than the standard Zeeman splitting. This is known as giant Zeeman splitting.

The same scenario might occur in semiconducting graphene ribbons with magnetic vacancies. When the inter-defect distance is larger than the critical spacing, D_c , the local moments are independent. Application of

a magnetic field aligns them and induces an exchange-induced splitting of the conduction and valence bands much larger than the intrinsic Zeeman splitting⁵². In the case of graphene ribbons with vacancies we have computed the spin splitting of the bottom of the conduction band

$$\delta \equiv E_{\uparrow} - E_{\downarrow}, \quad (10)$$

where E_{σ} is the first level above the mid-gap state [see Fig. 6(c)]. Notice that the shift of the top of the valence band and the bottom of the conduction band is such that the gap, ignoring the midgap states, is *spin-independent*. Since we consider independent defects, the calculation is done with a single defect per unit cell. In Fig. 11 we plot δ as a function of the inter-defect distance considering only values bigger than D_c for which the defects are decoupled. For a $U = 2\text{eV}$ we find that δ ranges between 5 and 15 meV. This splitting could be obtained with an applied magnetic field such that $g\mu_B B \gg kT$, yet, $\delta \gg g\mu_B B$. As in the case of real DMS, this giant Zeeman splitting scales linearly with the defect density, as shown in the inset of the right panel of Fig. 11. Since there is a maximal density above which the local moments are coupled and eventually they vanish, the splitting δ can not be increased indefinitely. This phenomenon also has an analog in DMS: Direct antiferromagnetic coupling between Mn spins eventually blocks the paramagnetic coupling to the external field.

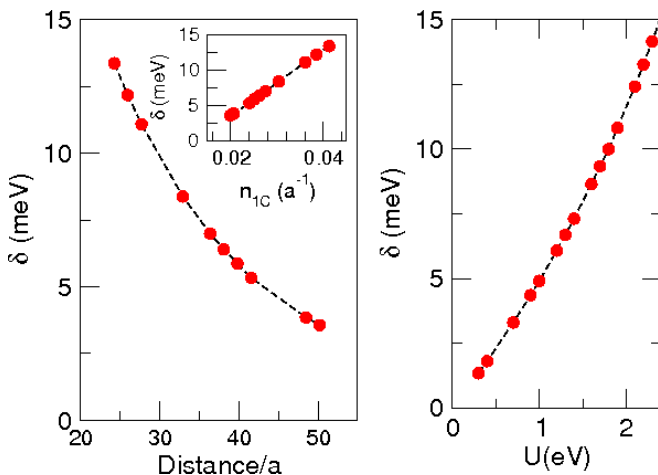


FIG. 11: (Color online) Left panel: Bottom of the conduction band spin splitting, δ , as a function of the defect distance and as a function of the linear defect density (inset) for a ribbon with $W = 7a$ and $U = 2\text{eV}$. Right panel: δ for the same ribbon for a fixed defect density as a function of U .

In the right panel of Fig. 11 we plot δ as a function of U . For small U we find that δ is almost linear with U . This can be understood in the framework of the analytical model discussed above. If we consider that, to lowest order, the magnetization only comes from the mid-gap states with wave function $\phi_v(i)$ and we compute the

splitting of the bottom of the conduction band states to first order perturbation theory, we obtain:

$$\delta = U \sum_i |\phi_c(i)|^2 \sum_v |\phi_v(i)|^2 \quad (11)$$

where $\phi_c(i)$ is the $U = 0$ single particle state of the bottom of the conduction band. If we approximate $\phi_c \simeq 1/\sqrt{N}$, where N is the number of atoms in the unit cell, and we use the normalization condition of the midgap states, $\sum_i |\phi_v(i)|^2 = 1$ then we have:

$$\delta \simeq \frac{UN_v}{N} \quad (12)$$

where N_v is the number of magnetic vacancies per unit cell. This equation accounts also for the fact that δ scales linearly with the defect density. Deviations from the linear behaviour arise due to the magnetization that arises from states other than mid-gap states.

The strong sensitivity of the conduction states of the defective armchair ribbon on the application of a moderate magnetic field should give rise to strong spin-dependent magnetotransport and magneto-optic effects, in analogy with DMS spintronic devices. Notice that, in contrast to standard Mn doped II-VI semiconductors, for which electrical injection of carriers results in a new carrier mediated coupling^{53,54}, the addition of carriers in this system would result in the compensation of the mid-gap states and the disappearance of the local moments, as shown in Fig. 8.

VI. DEFECTS IN BULK GRAPHENE: VACANCIES

So far we have considered the electronic structure of semiconducting graphene ribbons with vacancies and voids. As shown in Fig. 10 the critical distance for the quenching of the magnetic moments increases with the ribbon width. An important question is whether or not this critical distance converges to a finite value in the two-dimensional limit. We have also seen in Fig. 7(d) how the (standard deviation of the) magnetization Σ associated with vacancies decreases as the gap of the ribbon decreases. In this section we address the question of what happens to these and other results obtained above in the limit of infinitely wide ribbons where the gap goes to zero, i.e., bulk graphene. The extrapolation to the two-dimensional case is not straightforward. We thus consider a new strategy. Here we consider unit cells with periodic boundary conditions in both directions. An infinite graphene crystal with a unit cell formed by N_y parallel armchair-like chains, each of them containing N_x carbon atoms. The dimension of this unit cell is $(N_x \frac{\sqrt{3}}{4} a, N_y a)$ being a the graphene lattice parameter. We are interested in square unit cells and therefore we consider unit cells (N_x, N_y) of sizes (24,10), (32,13), (40,16), (48,20), (60,26), and (72,31). We locate one or more vacancies

in the unit cell considered and, as for ribbons, we obtain the eigenvalues, eigenfunctions, and the magnetization at each place of the system, $\langle m(i) \rangle$, by solving self-consistently the Hamiltonian.

A. System with vacancies of the same type

We locate a vacancy at the center of the unit cell in such a way that our system describes a square lattice of vacancies all located on the same type of atoms, e.g., B in our notation. We obtain that, in agreement with Lieb's theorem, the ground state of the system has a magnetic moment $S = 1/2$ per vacancy. We also obtain the spin gap of the system Δ_S , the wavefunction $\phi_v(i)$ of the first empty state, and the local magnetization. In the limit of a large unit cell $\Delta_S/2$ and $\phi_v(i)$ should be the energy and the wavefunction, respectively, of an isolated vacancy. In two dimensions we can characterize the linear size of the vacancy wavefunction by its first moment

$$\langle R \rangle = \sum_i |\mathbf{r}_i - \mathbf{r}_0| |\phi_v(i)|^2, \quad (13)$$

where \mathbf{r}_0 is the position of the vacancy and the sum is over all atoms of the unit cell. As discussed above, the bipartite character of the graphene lattice produces an antiferromagnetic coupling between the magnetization of the two sublattices of the system^{48,49}. We define the linear size of the magnetization in each sublattice as

$$M_d^{A(B)} = \sum_{i \in A(B)} |\mathbf{r}_i - \mathbf{r}_0| \langle m_i \rangle. \quad (14)$$

M_d^A and M_d^B have opposite signs, and their sum, $M_d = M_d^A + M_d^B$ indicates the extension of the net magnetization.

In Fig. 12 we plot the linear size of the vacancy wavefunction and of the magnetization as function of the distance between vacancies for different values of U . The first thing to note is that the size of the wavefunction increases linearly with the size of the unit cell, practically independent of the value of U . This result indicates that the electron-electron interaction almost does not affect ϕ_v which, when $U = 0$, becomes a quasilocalized state with weight in only one sublattice (A) and decays as $1/r$, in agreement with analytical results⁵¹. When $U = 0$ only the sublattice A is magnetized and $M_d = M_d^A$. However, M_d is considerable smaller than $\langle R \rangle$, indicating that the presence of the vacancy does not just creates a quasilocalized state, but also modifies strongly the wavefunctions of the states in the continuum. Notice the difference with the ribbons where the magnetization follows the wavefunction for sizable confinement gaps.

As we increase U , the magnetic texture evolves in such a way that their size M_d , as defined in Eq. (14), decreases. This is accompanied by an increase of the staggered magnetization, reflecting the antiferromagnetic

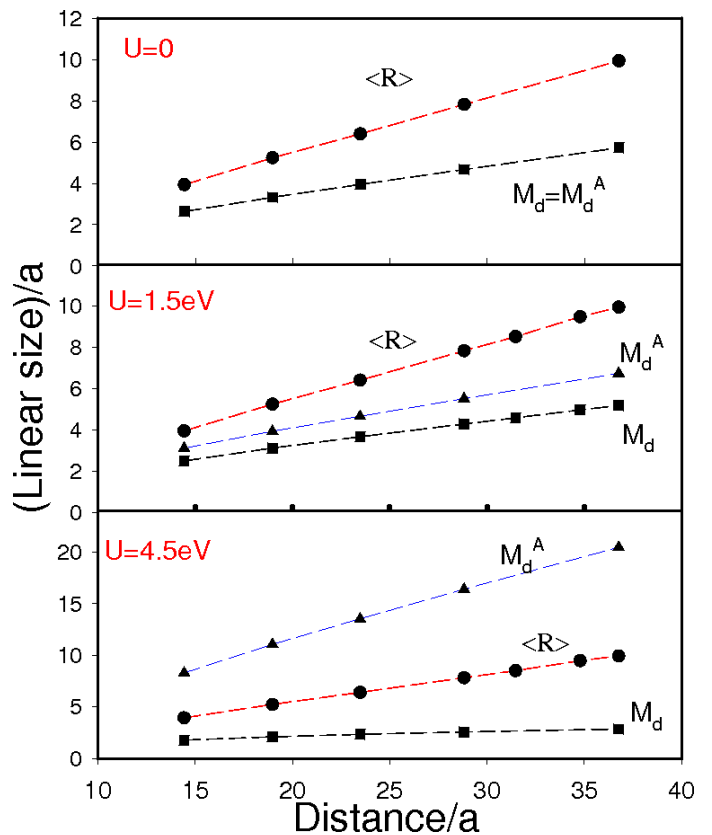


FIG. 12: (Color online) Linear size of the wavefunction of the vacancy, $\langle R \rangle$, of the net magnetization, M_d , and of magnetization in the sublattice A, M_d^A , as function of the distance between vacancies. From top to bottom the panels correspond to Hubbard constant, $U = 0$, $U = 1.5$ and $U = 4.5$ eV. The vacancies are located in sites type B.

tendency of the bipartite lattice, which polarizes the sublattice B in the opposite direction that sublattice A with $M_d^A > M_d$. This effect can be rather dramatic for moderate values of U , in Fig. 12 we show that for $U = 4.5$ eV the extension of the magnetization in sublattice A is considerable larger than $\langle R \rangle$ and M_d . Note that $U = 4.5$ eV is still below the critical value $U_{AF} \sim 5.5$ eV for the occurrence of an antiferromagnetic instability in perfect graphene^{10,55,56}. Thus, a network of vacancies in the same sublattice would have a magnetic ground state, in agreement with Lieb theorem, and enhanced staggered magnetization, compared to perfect graphene.

We now consider the midgap spin splitting Δ_S in two dimensional graphene with a finite density of vacancies in the same sublattice. In the previous case of semiconducting ribbons there was a strong indication that $E_g > \Delta_S$ for any ribbon width in the single vacancy limit. Hence, we might expect that Δ_S vanishes in two dimensional graphene. When we have a finite density of defects, Δ_S has also an inter-defect contribution arising from the hopping term. This mechanism is possible only if the midgap states have weight on the two sublattices. Midgap states associated with defects in the same sublattice can only be

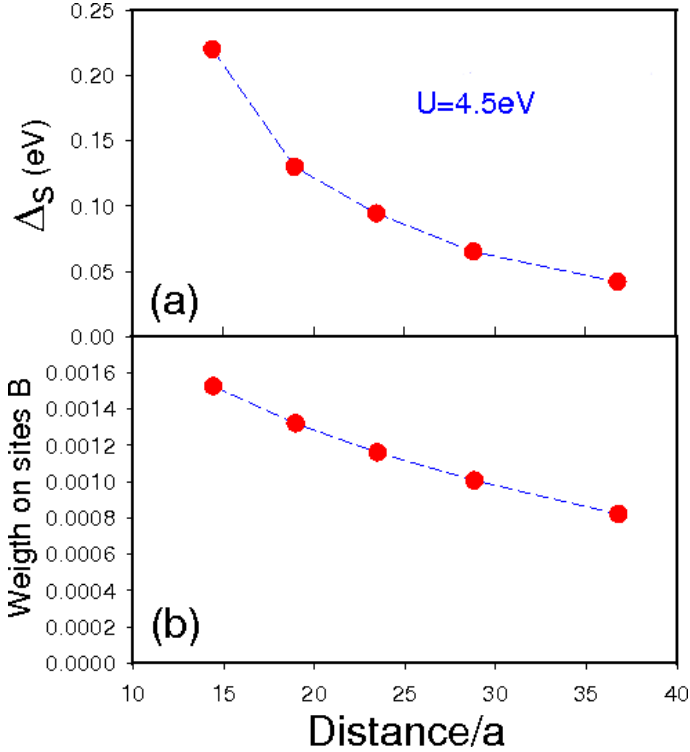


FIG. 13: (Color online) (a) Midgap spin splitting as function of the distance between vacancies and (b) weight of the quasilocized wavefunction on sites B. The vacancies are located in the sublattice B and $U = 4.5$ eV.

coupled through interaction driven sublattice mixing. As the gap is a product of the coupling between the magnetizations induced by the Hubbard interaction, the value of the gap increases quadratically with U to lowest order. Our calculations in Fig. 13(a) show that for $U \neq 0$, the midgap spin splitting Δ_S goes to zero as the density of vacancies goes to zero. In Fig. 13(b) we plot the weight of $\phi_v(i)$ on the sublattice where the vacancy is located. This quantity also tends to zero as the density of defects decreases. Thus, in the single impurity limit the spin gap goes to zero and the interacting $\phi_v(i)$ lives only on one sublattice.

B. Vacancies on different sublattices: Compensated case

In principle, one could expect that in real graphene samples the number of vacancies on sublattices A and B are roughly equal. In this situation Lieb's theorem requires that the total spin of the system should be essentially zero. From the results in the case of ribbons one should expect an antiferromagnetic coupling between the magnetic moments for small concentrations of vacancies. For large concentrations the local magnetic moments should disappear and the sample should turn non-magnetic. In order to study the interaction between va-

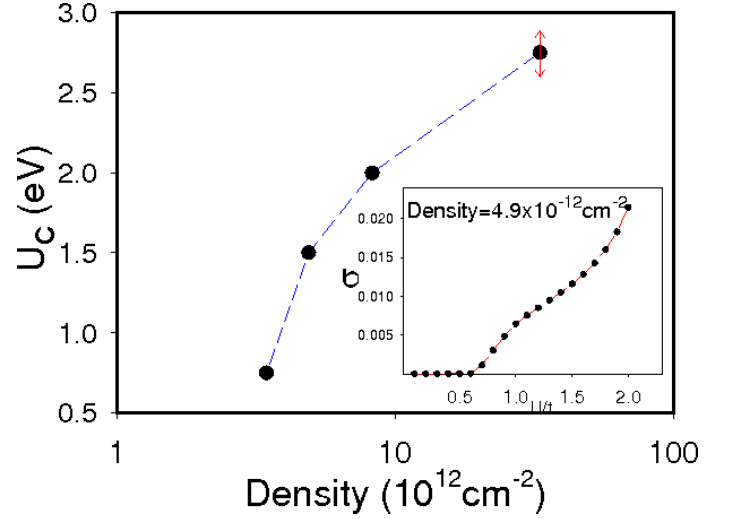


FIG. 14: (Color online) Value of the critical values for the occurrence of a magnetic texture in a system of vacancies on atoms of type A and B forming two square lattice interpenetrated lattices. The inset indicates the variation of the standard deviation of the local magnetizations as function of the Hubbard constant for a system of dimension (26,60). The error bar is an estimation of the numerical error in the calculations.

cancies located in different sublattices and the local magnetization in a compensated system, we locate two vacancies with total sublattice imbalance equal to zero in the unit cell. The A and B impurities form two interpenetrated square lattices in such a way that the distance between impurities is maximum. We have checked that in agreement with Lieb's theorem the $S=0$ solution is the ground state of the system.

We quantify the local magnetization studying the standard deviation of $\langle m_i \rangle$,

$$\sigma = \sqrt{\frac{\sum_i \langle m_i \rangle^2}{N}}, \quad (15)$$

where the sum is over all carbon atoms and $N=N_x \times N_y$ is the number of atoms in the unit cell. In the inset of Fig. 14 we plot σ as a function of U for a unit cell of size (26, 60), which corresponds to a density of vacancies of $0.5 \times 10^{13} \text{ cm}^{-2}$. We obtain that for small values of U the magnetization is zero everywhere and that there is a critical value of the Hubbard coupling, U_c , for which a local magnetization near the vacancies appears¹⁰. This critical U depends on the density of vacancies, and in Fig. 14 we plot U_c as function of the density of vacancies. We obtain that U_c decreases with the density of vacancies and from our results we conclude that in the limit of zero density U_c tends to zero. In that limit, each vacancy hosts a spin one half texture, which is decoupled from the others. For high density of vacancies and moderate values of U , the kinetic energy coupling between the vacancies is stronger than the electronic repulsion, and in order to minimize the energy the system makes

the local magnetization zero everywhere. When the density of impurities decreases, the kinetic energy coupling between vacancies decreases and eventually the impurities become uncoupled and each of them gets a total spin $\pm 1/2$ and the system behaves as a diluted antiferromagnetic system⁴⁸. Unless a reason for global lattice imbalance exists (unknown to us), for realistic values of U in the range $1 < U < 2$ eV³ we expect that in highly irradiated graphene samples the local magnetization should be zero across the sample.

VII. DISCUSSION AND CONCLUSIONS

Some of the possible limitations of our approach have already been mentioned in the beginning. We have left aside the issue of the structural stability of passivated vacancies and voids. Away from the edges, a single monoatomic vacancy might not result in a local atomic configuration that can be described with our model. On the other side, the effect of a hydrogen atom atop a carbon atom on graphene is very similar to the one described by our model¹¹. Hence, the anomalous magnetic behaviour of irradiated graphite might be related to $H - C$ pairs, rather than to missing atoms. It is also important to signal that the mean field approximation is known to overestimate the appearance of magnetic order and yield critical values of U/t smaller than those obtained with methods that include quantum fluctuations⁵⁵. Finally, we have neglected both second neighbor hopping and interatomic Coulomb repulsions. Interestingly, both DFT and mean field Hubbard model yield a very similar description of the magnetic behaviour of graphene islands³ and zigzag graphene ribbons³⁷. This indicates that the couplings neglected in the simple Hubbard model have a small effect on the low energy electronic structure that dominates the physical properties.

We now summarize the main conclusions of this work. In the context of our model, the main results are:

1. The electronic properties of the defects arising from the removal of atoms from graphene depend dramatically on an integer number, the sublattice imbalance (or imbalance charge) $N_I = N_A - N_B$, which counts the difference in the total number of atoms per sublattice removed from a perfectly balanced graphene lattice. N_I can take values $0, \pm 1, \pm 2$ etc.
2. It can be rigorously shown²⁸ that the single-particle spectrum of a structure with sublattice imbalance N_I has, at least, $|N_I|$ midgap states per spin channel, occupied by $|N_I|$ electrons in neutral graphene.
3. Repulsive Coulomb interactions will result in a many-body ground state with $2S = |N_I|$. This is an exact result in the case of the Hubbard model³².
4. Whereas the global electronic structure of a given graphene system is given by the Lieb, the local

structure is not. By assigning *local* sublattice imbalance numbers to defects, provided that they are sufficiently apart, a set of rules to predict basic features of the magnetic structure has been proposed.

5. We find that single voids with $|N_I = 1|$ give rise to states with spin-charge separation, in the sense that a localized magnetic texture does not entail charge localization. The addition of a single electron to the system results in a many-body state with $S = 0$ and the disappearance of the magnetic texture, which is substituted by a charge texture, as seen in Fig. 8. In this sense, the properties of these states are very similar to Su-Schrieffer-Heeger midgap states⁴⁵.
6. The addition rules for two voids with a given local sublattice imbalance or imbalance charge present similarities with those of vortices, e.g., in superconductors. When sufficiently apart, two voids with local imbalance $+N_I$ and $-N_I$ behave like two independent objects with local spin $2S = |N_I|$. Below a certain distance they annihilate each other and the local magnetization vanishes (Fig. 10). When two voids with the same sign are brought together, they result in a region with enhanced local magnetization and spin $2S = |N_I| + |N_I|$, as seen in Fig. 2.
7. In analogy with graphene nanoislands³, sufficiently large voids with $N_I = 0$ can still have local magnetic moments. These can be interpreted as if the large void with $N_I = 0$ was the sum of two voids with $\pm N_I'$. An example of this is the rhomboid of Fig. 9, obtained from merging two triangular voids with $N_I = \pm 3$ back to back.
8. Our results show that spin interactions between two magnetic defects of same $|N_I|$ can be of three types: Ferromagnetic, antiferromagnetic or annihilating. In the first case, the ground state spin is the sum of the spins of the magnetic defects when infinitely apart, in the second case the spin is the difference between those two. In the third case both the total and the local spins are zero. Antiferromagnetic and annihilating couplings occur in lattices without global sublattice imbalance, whereas ferromagnetic coupling requires global sublattice imbalance.
9. Our simulations show that, in balanced defective structures, there is a maximal density of monoatomic vacancies that can sustain local moments. In the case of ribbons, this critical density depends on the ribbon width. The critical density also depends on U . A phase diagram for bulk graphene is provided in Fig 14.
10. Depending on the density of vacancies, distributed randomly in the two sublattices, we distinguish three phases. In the very dilute limit the system is paramagnetic, with some common properties with II-VI diluted magnetic semiconductors.

In the opposite high-density limit the local moments are annihilated. The intermediate phase features antiferromagnetically coupled local moments. This would be a realization of the so-called diluted antiferromagnet⁴⁸

11. We predict giant Zeeman splitting in the case of semiconducting ribbons in the dilute limit. Upon application of an external magnetic field such that $g\mu_B H > k_B T$, the magnetic moment of all the defects would point parallel to applied field. This would result in a interaction induced splitting in the band states, much larger than the ordinary Zeeman splitting, as seen in Fig. 11.
12. A ferromagnetic phase is not expected for defective graphene, unless vacancies occur predominantly in one of the two sublattices. Such an unbalanced situation would require further explanation.
13. In the case of zero-gap graphene, we find that

midgap states survive, even in the interacting case, in the very dilute limit (Fig. 13). Since ideal graphene is a semimetal, the thermodynamics properties of graphene might be dominated by this type of defects.

Upon completion of this manuscript, a related work by O. V. Yazyev (aXiv:0802.1735) has been reported.

VIII. ACKNOWLEDGEMENTS

We acknowledge fruitful discussions with F. Guinea, B. Korgel, and P. López-Sancho. This work has been financially supported by MEC-Spain under Grants Nos. MAT2007-65487, MAT2006-03741, and CONSOLIDER CSD2007-00010, and by Generalitat Valenciana under Grant No. ACOMP07/054.

-
- ¹ J. M. D. Coey, *Solid State Science* **7**, 660 (2005).
 - ² H. Ohldag, T. Tyliczszak, R. Hohne, D. Spemann, P. Esquinazi, M. Ungureanu, and T. Butz, *Phys. Rev. Lett.* **98**, 187204 (2007).
 - ³ J. Fernández-Rossier and J. J. Palacios *Phys. Rev. Lett.* **99**, 177204 (2007).
 - ⁴ R. C. Longo and L. J. Gallego, *Phys. Rev. B* **74**, 193409 (2006).
 - ⁵ W. Luo, S. J. Pennycook, S. T. Pantelides, *Nano Lett.* **7**, 3134 (2007).
 - ⁶ P. Crespo, R. Litrán, T. C. Rojas, M. Multigner, J. M. de la Fuente, J. C. Sánchez-López, M. A. García, A. Hernando, S. Penadés, and A. Fernández, *Phys. Rev. Lett.* **93**, 087204 (2004).
 - ⁷ Y. Yamamoto, T. Miura, M. Suzuki, N. Kawamura, H. Miyagawa, T. Nakamura, K. Kobayashi, T. Teranishi, and H. Hori, *Phys. Rev. Lett.* **93**, 116801 (2004).
 - ⁸ P. O. Lehtinen, A. S. Foster, Y. Ma, A. V. Krasheninnikov, and R. M. Nieminen, *Phys. Rev. Lett.* **93**, 187202 (2004)
 - ⁹ M. A. H. Vozmediano, M. P. Lopez-Sancho, T. Stauber, F. Guinea, *Phys. Rev. B* **72**, 155121 (2005).
 - ¹⁰ H. Kumazaki and D. S. Hirashima, *J. Phys. Soc. Jpn.* **76**, 064713 (2007).
 - ¹¹ Oleg V. Yazyev and Lothar Helm, *Phys. Rev. B* **75**, 125408 (2007).
 - ¹² T. Chanier, I. Opahle, M. Sargolzaei, R. Hayn, and M. Lannoo, *Phys. Rev. Lett.* **100**, 026405 (2008).
 - ¹³ K. S. Novoselov *et al.*, *Science* **306**, 666 (2004).
 - ¹⁴ J. Scott-Bunch *et al.*, *Nano Lett.* **5**, 287 (2005).
 - ¹⁵ K. S. Novoselov, A. K. Geim, S. V. Morozov, D. Jiang, M. I. Katsnelson, I. V. Grigorieva, S. V. Dubonos and A. A. Firsov, *Nature* **438**, 197 (2005).
 - ¹⁶ Y Zhang, Y. W. Tan, H. L. Stormer, and P. Kim, *Nature* **438**, 201 (2005).
 - ¹⁷ C. Berger *et al.*, *Science* **312**, 1191 (2006).
 - ¹⁸ K. S. Novoselov, Z. Jiang, Y. Zhang, S. V. Morozov, H. L. Stormer, U. Zeitler, J. C. Maan, G. S. Boebinger, P. Kim, and A. K. Geim, *Science* **315**, 1379 (2007).
 - ¹⁹ A. Geim and K. Novoselov, *Nature Materials* **6**, 183 (2007).
 - ²⁰ Zhihong Chen, Yu-Ming Lin, Michael J. Rooks, and Phaedon Avouris, *Physica E: Low-dimensional Systems and Nanostructures*, **40/2**, 228, (2007).
 - ²¹ M. Y. Han, B. Ozyilmaz, Y. Zhang, and P. Kim, *Phys. Rev. Lett.* **98**, 206805 (2007).
 - ²² B. Ozyilmaz, P. Jarillo-Herrero, D. Efetov, D. A. Abanin, L. S. Levitov, P. Kim, *Phys. Rev. Lett.* **99**, 166804 (2007).
 - ²³ L. A. Ponomarenko, F. Schedin, M. I. Katsnelson, R. Yang, E. H. Hill, K. S. Novoselov, A. K. Geim, arXiv:0801.0160.
 - ²⁴ J. Wu, W. Pisula, and K. Mullen, *Chem. Rev.*, **107**, 718 (2007).
 - ²⁵ A. L. Vázquez de Parga *et al.*, *Phys. Rev. Lett.* **100**, 056807 (2008).
 - ²⁶ R. Saito, M. S. Dresselhaus, and G. Dresselhaus, *Physical Properties of Carbon Nanotubes*, (Imperial College Press, London, 1998).
 - ²⁷ P. K. Wallace, *Phys. Rev.* **71**, 622 (1947).
 - ²⁸ M. Inui, S. A. Trugman, and E. Abrahams, *Phys. Rev. B* **49**, 3190 (1994).
 - ²⁹ Gerardo G. Naumis, *Phys. Rev. B* **76**, 153403 (2007).
 - ³⁰ V. M. Pereira, J. M. B. Lopes dos Santos, A. H. Castro Neto, arXiv:0712.0806.
 - ³¹ H. C. Longuet-Higgins, *The Journal of Chemical Physics* **18**, 265 (1950).
 - ³² Elliott H. Lieb, *Phys. Rev. Lett.* **62**, 1201 (1989).
 - ³³ K. Wakabayashi, M. Sigrist, and M. Fujita, *J. Phys. Soc. Jpn.* **67**, 2089 (1998).
 - ³⁴ Y.-W. Son, M. L. Cohen, and S. G. Louie, *Phys. Rev. Lett.* **97**, 216803 (2006).
 - ³⁵ Young-Woo Son, M. L. Cohen, and S. G. Louie, *Nature (London)* **444**, 347 (2006).
 - ³⁶ L. Pisani, J. A. Chan, B. Montanari, and N. M. Harrison, *Phys. Rev. B* **75**, 064418 (2007).
 - ³⁷ J. Fernández-Rossier, arXiv:0710.3484 (*Phys. Rev. B* in press).
 - ³⁸ K. Nakada, M. Fujita, G. Dresselhaus, and M. S. Dresselhaus, *Phys. Rev. B* **54**, 17954 (1996).

- ³⁹ L. Brey and H. A. Fertig, Phys. Rev. B **73**, 235411 (2006).
- ⁴⁰ F. Muñoz-Rojas, D. Jacob, J. Fernández-Rossier, and J. J. Palacios, Phys. Rev. B **74**, 195417 (2006).
- ⁴¹ S. Reich, J. Maultzsch, C. Thomsen, and P. Ordejón, Phys. Rev. B **66**, 035412 (2002).
- ⁴² M. P. López-Sancho, M. C. Muñoz, and L. Chico, Phys. Rev. B **63**, 165419 (2001).
- ⁴³ J. Fernández-Rossier, J. J. Palacios, L. Brey Phys. Rev. B. **75**, 205441 (2007).
- ⁴⁴ F. Muñoz-Rojas, J. Fernández-Rossier, L. Brey, and J. J. Palacios, Phys. Rev. B **77**, 045301 (2008).
- ⁴⁵ W. P. Su, J. R. Schrieffer, and A. J. Heeger, Phys. Rev. Lett. **42**, 1698 (1979).
- ⁴⁶ O. Hod, J. E. Peralta, and G. E. Scuseria, Phys. Rev. B **76**, 233401 (2007); O. Hod, V. Barone, and G. E. Scuseria, Phys. Rev. B **77**, 035411 (2008).
- ⁴⁷ L. Pisani, B. Montanari, and N. M. Harrison, arXiv:0710.0957.
- ⁴⁸ L. Brey, H. A. Fertig, and S. Das Sarma, Phys. Rev. Lett. **99**, 116802 (2007).
- ⁴⁹ Saeed Saremi, Phys. Rev. B **76**, 184430 (2007).
- ⁵⁰ W. L. Wang, S. Meng, and E. Kaxiras, Nano Lett. **8**, 241 (2008); O. V. Yazyev, W. L. Wang, S. Meng, and E. Kaxiras, Nano Lett. **8**, 766 (2008).
- ⁵¹ Vitor M. Pereira, F. Guinea, J. M. Lopes dos Santos, N. M. Peres, and A. H. Castro Neto, Phys. Rev. Lett. **96**, 036801 (2006).
- ⁵² J. K. Furdyna, J. Appl. Phys. **64**, R29 (1988).
- ⁵³ H. Boukari, P. Kossacki, M. Bertolini, D. Ferrand, J. Cibert, S. Tatarenko, A. Wasiela, J. A. Gaj, and T. Dietl, Phys. Rev. Lett. **88**, 207204 (2002).
- ⁵⁴ J. Fernández-Rossier and L. Brey, Physical Review Letters **93**, 117201 (2004).
- ⁵⁵ S. Sorella and E. Tosatti, Europhys. Lett. **19**, 699 (1992).
- ⁵⁶ N. Peres, M. A. N. Araujo, D. Bozi, Phys. Rev. B **70**, 195122 (2004).